

Predicting Neo-Adjuvant Chemotherapy Response in Triple-Negative Breast Cancer Using Pre-Treatment Histopathologic Images

Hikmat Khan^{1*}, Ziyu Su¹, Huina Zhang², Yihong Wang³, Bohan Ning⁴, Shi Wei⁴, Hua Guo⁴, Zaibo Li¹, and Muhammad Khalid Khan Niazi¹

1 Department of Pathology, College of Medicine, The Ohio State University Wexner Medical Center, Columbus, OH, USA

2 Department of Pathology, University of Rochester Medical Center, Rochester, NY 14642, USA

3 Department of Pathology and Laboratory Medicine, Warren Alpert Medical School of Brown University, Lifespan Academic Medical Center, Providence, RI, 02903, USA

4 Department of Pathology, University of Alabama at Birmingham, Birmingham, AL, USA

* **Correspondence:** Hikmat.khan@osumc.edu

Abstract

Triple-negative breast cancer (TNBC) is an aggressive subtype defined by the lack of estrogen receptor (ER), progesterone receptor (PR), and Human Epidermal Growth Factor Receptor 2 (HER2) expression, resulting in limited targeted treatment options. Neoadjuvant chemotherapy (NACT) is the standard treatment for early-stage TNBC, with pathologic complete response (pCR) serving as a key prognostic marker; however, only 40–50% of patients with TNBCs achieve pCR. Accurate prediction of NACT response is crucial to optimize therapy, avoid ineffective treatments, and improve patient outcomes. In this study, we developed a deep learning model to predict NACT response using pre-treatment hematoxylin and eosin (H&E)-stained biopsy images. Our model achieved promising results in five-fold cross-validation (accuracy: 82%, AUC: 0.86 F1-score: 0.84, sensitivity: 0.85, specificity: 0.81, precision: 0.80). Through analysis of model attention maps in conjunction with multiplexed immunohistochemistry (mIHC) data revealed that regions of high predictive importance consistently colocalized with tumor areas showing elevated PD-L1 expression, CD8+ T-cell infiltration, and CD163+ macrophage density – all established biomarkers of treatment response. Our findings indicate that incorporating IHC-derived immune profiling data could substantially improve model interpretability and predictive performance. Furthermore, this approach may accelerate the discovery of novel histopathological biomarkers for NACT and advance the development of personalized treatment strategies for TNBC patients.

Keywords: Triple-negative breast cancer (TNBC), Neoadjuvant chemotherapy (NACT), Pathologic complete response (pCR), Artificial Intelligence (AI), Treatment response prediction

1. Introduction

Triple-negative breast cancer (TNBC) is a highly aggressive and clinically challenging subtype of breast cancer, characterized by the lack of estrogen receptor (ER), progesterone receptor (PR), and Human Epidermal Growth Factor Receptor 2 (HER2) overexpression and/or gene amplification [1-5]. Due to absence of ER, PR and HER2 expression, TNBC lacks effective targeted therapies, leaving neoadjuvant chemotherapy (NACT) as an initial treatment for early-stage disease [6,7], with the primary objectives of achieving pathologic complete response (pCR ypT0N0, with no residual invasive carcinoma in the breast or lymph nodes) [8,9] (i.e., complete absence of residual invasive carcinoma) or downstaging tumors before surgical intervention, potentially improving surgical outcomes and allowing for breast-conserving surgery in cases that might otherwise require mastectomy [2,3][10]. Around 40–50% of patients achieve a pCR [3,11-15], a critical surrogate endpoint strongly correlated with prolonged disease-free and overall survival [16]. Conversely, patients with residual disease (non-pCR) face higher rates of relapse and worse overall survival [6,17], highlighting the urgent need for NACT prediction response to effectively guide the clinical decision-making by stratifying patients into distinct prognostic and therapeutic pathways, tailor therapies and avoid unnecessary treatments [18-20]. Furthermore, early identification of patients likely or unlikely to achieve pCR could support timely consideration of alternative therapies, optimize surgical planning, reinforce adherence to recommended treatment pathways and spare patients from the toxicities of ineffective chemotherapy [16,21]. However, the aggressive biology of TNBC and the lack of reliable predictive biomarkers for NACT response in routine clinical practice make precise prediction of treatment outcomes a major unmet need with significant clinical implications [15,18,22-25].

Many studies have explored whether standard clinicopathological features—such as tumor size, histologic grade, subtype, and lymph node involvement—can predict response to NACT, though findings remain inconsistent [26]. While some research suggests that smaller, lower-grade, node-negative (N0) tumors are more likely to achieve a pCR, others report no significant correlation, indicating these factors alone are insufficient for reliable prediction [27-34]. Lacking universally approved biomarker to predict NACT response of TNBC underscore the need for more robust predictive tools beyond conventional clinical markers. Recent advances in artificial intelligence (AI), particularly deep learning, have opened new avenues for predicting the response to NACT. Several studies leverage radiomics and deep learning due to its high soft-tissue contrast. For instance, Zhou et al. [35] utilized multiparametric MRI (DCE-MRI and DWI) with deep learning, achieving an AUC of 0.86, suggesting that early treatment-phase imaging may capture predictive signatures. Similarly, Golden et al. [36] reported a modest AUC of 0.68, possibly due to smaller sample sizes (n=60) or feature selection methods. Alternatively, Jiang et al. [37] employed ultrasound-based radiomics and deep learning to predict NACT response in 592 TNBC patients,

achieving an AUC of 0.93 and an accuracy of 0.84. Several studies combined imaging with clinical variables to improve accuracy. For instance, Xu et al. [38] integrated MRI with clinicopathological data (AUC=0.76), while Jimenez et al. [39] incorporated tumor-infiltrating lymphocytes (TILs) (AUC=0.71). These results suggest that hybrid models may better capture tumor heterogeneity, though interpretability remains a challenge.

While prior studies have predominantly relied on radiomics or clinical imaging for predicting NACT response in TNBC, histopathology-driven AI models remain underexplored despite their clinical ubiquity and cost-effectiveness. Recently, Savitri et al. [40] pioneered deep learning on H&E-stained slides (AUC=0.75), offering a cost-effective alternative to imaging. Huang et al. [41] introduced IMPRESS, an AI-based pipeline combining H&E and multiple immunohistochemistry (mIHC) (PD-L1/CD8+/CD163+), achieving an AUC of 0.8975 for HER2+ and 0.7674 for TNBC, demonstrating that AI-based methods can outperform manual pathologist assessments in predicting NAC response. Hussain et al. [42] explore deep learning advancements in biomarker discovery and multi-omics integration to enhance TNBC management, while highlighting challenges such as model interpretability and limited data availability, and emphasizing the importance of multidisciplinary collaboration and continued research. In this study, we develop a deep learning-based method to predict pCR directly from pre-treatment H&E-stained biopsy images in a cohort of 174 TNBC patients. Our model achieves promising results in predicting the NACT response in TNBC (accuracy: 82%, AUC: 0.86 F1-score: 0.84, sensitivity: 0.85, specificity: 0.81, precision: 0.80). We visualize the deep learning model's attention maps, which localize predictive histological hotspots in H&E slides, with two goals: (1) to enhance model interpretability and (2) to support biomarker discovery by correlating these regions with available mIHC data from a subset of patients. Notable, the attention maps highlight biologically relevant tumor microenvironment (TME) features—including PD-L1 expression, CD8+ T cells, and CD163+ macrophages—providing both predictive power and mechanistic insights. Furthermore, our visual analysis of these attention hotspots across H&E and mIHC images reveals the model's focus on TME components-including PD-L1 expression, CD8+ T cells, and CD163+ macrophages, known to be associated with NACT response [25]. Suggesting that multimodal analysis could: (1) further enhance predictive performance, (2) elucidate TME-specific response mechanisms, and (3) accelerate the development of clinically actionable biomarkers for precision oncology in TNBC.

2. Methods

2.1. Study Population

In this retrospective study, a cohort of 174 female patients diagnosed with TNBC and treated with NACT at The Ohio State University Wexner Medical Center (2013–2020). All patients had documented treatment outcomes, with 81 achieving a pCR and 93 categorized as non-pCR. Among them, 64 patients had available pre-NACT mIHC images paired with corresponding H&E-stained images. The study was approved by the Institutional Review Board (IRB Protocol #2016C0025).

2.2. Dataset

We employed the 174 H&E-stained whole-slide images (WSIs), all derived from pre-neoadjuvant chemotherapy (pre-NAC) biopsy specimens containing tumors larger than 0.1cm, along with their corresponding NACT response outcomes (pCR vs. non-pCR) to train the deep learning model using a five-fold cross-validation strategy. To ensure generalizability, the dataset was split at the patient level in each fold with stratified sampling, maintaining balanced pCR or non-pCR ratios of across training, validation, and test sets. The training split was used to train the model, validation sets guided hyperparameter tuning and early stopping to mitigate overfitting, while the test set was used to perform the fold-level evaluation.

2.3. Methodology

We employed an attention-based multiple instance learning (MIL) framework to predict NACT response in TNBC using pre-treatment H&E biopsy images [43]. In this framework, each H&E-stained image is treated as a "bag" composed of smaller image patches (instances or tiles). While only the bag-level label (pCR vs. non-pCR) is known, individual patch labels are unavailable. The model learns to identify and attend to the most informative regions (patches) within each image that contribute to the overall prediction of pCR for NACT. The complete

pipeline, as illustrated in Figure 1, comprises four key stages: tissue patch extraction, patch-level feature extraction, attention-based feature aggregation, and slide-level classification.

2.3.1 Tissue Patching and Feature Extraction

Each H&E-stained image is partitioned into non-overlapping 512×512-pixel patches at 40× magnification (0.25 µm/pixel resolution). Each was then passed through a pre-trained UNI v2 [44], a computational pathology foundation model pretrained on 1.2 million histopathology slides, to extract discriminative feature vectors $h_i \in \mathbb{R}^d$, for each patch i , where $d=1536$ denotes the feature dimensionality [44,45].

2.3.2 Attention-Based Aggregation

An attention mechanism was employed to learn each patch weights (i.e., $\alpha_i \in [0,1]$, satisfying $\sum \alpha_i = 1$) [43], reflecting its importance in predicting the patient's overall NACT response (pCR or non-pCR). These weights are used to compute a slide-level feature vector z through attention-weighted aggregation:

$$z = \sum_{k=1}^N \alpha_k h_k,$$

where N is the number of patches in the given slide, h_k is the feature vector for the k -th patch, and α_k is the corresponding attention weight for k -th patch. The attention weights are computed as follows:

$$\alpha_k = \frac{\exp(w^T \tanh(Vh_k^T))}{\sum_{j=1}^N \exp(w^T \tanh(Vh_j^T))},$$

Where w and V are learnable parameters of the attention-based deep learning model, while α_k represents the normalized attention weight of k -th patch in the final prediction. The attention mechanism offers two key benefits: (1) it enhances predictive performance by adaptively focusing on the most relevant morphological features, and (2) it provides interpretability through spatial attention maps that highlight histological regions strongly associated with NACT response (see Figure 4, 5 and 6). Additionally, these attention weights hold the promise for revealing novel histopathological biomarkers, yielding insights for model refinement and to the discovery of clinically actionable insights for patient stratification.

2.3.3 WSI Classification (pCR Prediction)

The aggregated slide-level feature vector z is fed into a fully connected neural network to predict the likelihood of a pCR versus non-pCR response to NACT. A sigmoid activation function is applied to the final layer to generate a probability score representing the model's confidence in the pCR classification.

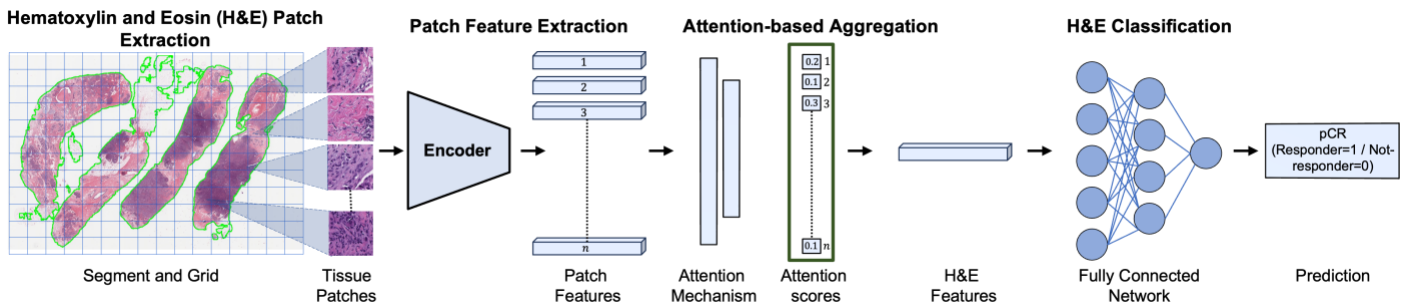


Figure 1: Overview of the pipeline for predicting pathologic complete response (pCR) to neoadjuvant chemotherapy (NACT) in triple-negative breast cancer (TNBC) using pre-treatment H&E-stained whole-slide biopsy images. First, H&E-stained images are segmented and divided into a grid to extract tissue patches. Each patch is then encoded into a feature vector using a pre-trained deep learning encoder (i.e. Uni v2 [44]). These patch-level features are aggregated using an attention mechanism [43], which assigns higher weights to the most informative regions. Finally, the aggregated slide-level features are passed through a fully connected neural network to classify each patient as either a pCR (responder) or non-pCR (non-responder) to NACT.

2.3.4 Class-weighted Loss Function

To mitigate class imbalance in dataset (81 pCR vs. 93 non-pCR cases), we employed a class-weighted binary cross-entropy loss function, defined as:

$$\mathcal{L} = -\frac{1}{B} \sum_{k=1}^B [w_{pCR} \cdot y_k \log p_k + w_{non-pCR} \cdot (1 - y_k) \log(1 - p_k)]$$

where B is the batch size (set to 1 in our case), $y_k \in \{0, 1\}$ is the ground-truth label (i.e. either pCR=1 or non-pCR=0), and p_k is the predicted probability for the k -th bag, while w_{pCR} and $w_{non-pCR}$ are class weights assigned to the pCR and non-pCR classes, respectively. The class weighting scheme compensates for the inherent imbalance in NACT response by assigning a higher penalty to misclassification of the minority class (i.e., pCR), thereby encouraging the model to be more sensitive to underrepresented cases during training.

2.3.5 Training and Implementation Details

All experiments were conducted in PyTorch on an NVIDIA A100 GPU (40GB VRAM). WSI were processed using the publicly available Trident library, extracting tissue patches at 40x magnification. Model training utilized the stochastic gradient descent (SGD) [46,47] optimizer with a learning rate of 1×10^{-4} and weight decay of 1×10^{-5} . All models were trained with a batch size of one, and a maximum of 1024 epochs, using early stopping with a patience of 50 epochs based on validation loss. To address the inherent class imbalance between pCR and non-pCR cases, a class-weighted binary cross-entropy loss was used, where class weights for the pCR and non-pCR classes were set inversely proportional to their frequencies in the training data, ensuring the model remained sensitive to the minority class. To mitigate model's overfitting risk, patch-level data augmentation was applied, including random rotation ($\pm 30^\circ$), color jitter (brightness, contrast, saturation, and hue adjustments of ± 0.2), and horizontal or vertical flipping [48]. These augmentation strategies were essential to mitigate overfitting risks inherent to medical imaging datasets with limited sample sizes [49].

3. Results and Discussion

Table 1 summarizes the five-fold cross-validation results. Our attention-based MIL model achieved strong and consistent predictive performance, with an average accuracy of 82% (± 0.02), area under the curve (AUC) of 0.86 (± 0.03), F1-score of 0.84 (± 0.04), sensitivity of 0.85 (± 0.06), specificity of 0.81 (± 0.01), and precision of 0.80 (± 0.05). These balanced metrics demonstrate the model's capacity to reliably identify both pCR and non-pCR cases, which is essential for clinical translation. Figure 2 and 3 displays the confusion matrices, AUC of Receiver Operating Characteristic (ROC) curves for each fold, respectively. Further, analysis of the confusion matrices (see Figure 2, and 3) reveals that false positives (predicting pCR when the patient did not achieve it) and false negatives (predicting non-pCR when the patient did achieve pCR) are relatively balanced across folds. This balanced error distribution is clinically desirable, as both misclassification types carry serious consequences: false negatives could deny patients effective NACT, while false positives could expose patients to unnecessary treatment toxicities without therapeutic benefit.

Table 1. Performance metrics for predicting pathologic complete response (pCR) versus non-pCR following neoadjuvant chemotherapy (NACT) in triple-negative breast cancer (TNBC) using five-fold cross-validation.

Metrics are reported for each fold (Folds 1–5), along with mean \pm standard deviation across all test folds, demonstrating consistent performance in accuracy, AUC, F1-score, sensitivity, specificity, and precision.

| Folds | Accuracy | AUC | F1-Score | Sensitivity | Specificity | Precision |
|--|----------|------|----------|-------------|-------------|-----------|
| 1 | 0.83 | 0.88 | 0.88 | 0.89 | 0.82 | 0.78 |
| 2 | 0.78 | 0.83 | 0.78 | 0.78 | 0.78 | 0.78 |
| 3 | 0.83 | 0.91 | 0.86 | 0.90 | 0.80 | 0.75 |
| 4 | 0.83 | 0.85 | 0.88 | 0.89 | 0.82 | 0.78 |
| 5 | 0.83 | 0.81 | 0.80 | 0.78 | 0.84 | 0.89 |
| <div>0.82\pm0.02 0.86\pm0.03 0.84\pm0.04 0.85\pm0.06 0.81\pm0.01 0.80\pm0.05</div> | | | | | | |

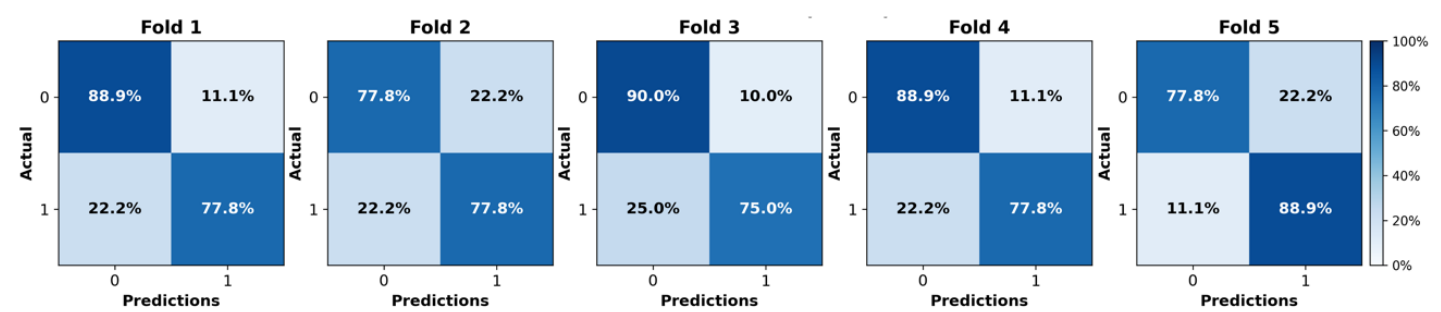


Figure 2. Confusion matrices illustrate the model’s performance on each test fold, highlighting the model’s balanced classification of pathologic complete response (pCR) and non-pCR cases.

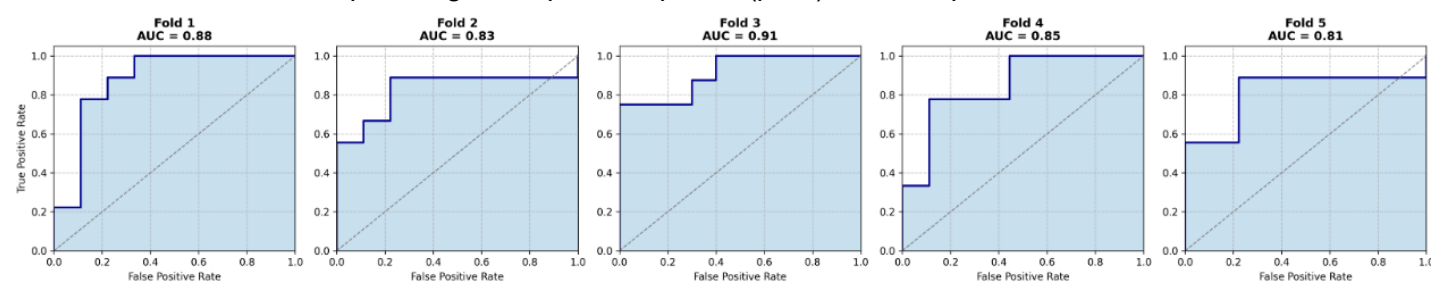


Figure 3. Receiver Operating Characteristic (ROC) curves for each test fold in five-fold cross-validation. AUC values range from 0.81 to 0.91, demonstrating the model’s robust and consistent classification performance across all folds.

3.1. Attention Maps Analysis and Corresponding Biological Insights

Figures 4 and 5 illustrate the high-attention (hotspot) regions identified by the model in representative pCR (responder) and non-pCR (non-responder) cases from the test set, demonstrating its ability to localize tumor regions prognostically relevant for NACT response prediction. A more detailed visual analysis of the model-highlighted regions in H&E-stained slides, alongside the corresponding areas in mIHC images for visual reference, revealed that the model primarily focused on the tumor microenvironment (TME), with regions enriched in key immune biomarkers, including PD-L1 (brown), CD8⁺ T-cell infiltration (green), and CD163⁺ macrophage populations (red) (see Figures 4 and 5). These findings not only enhance the model’s interpretability but also align with established literature showing that the tumor-associated macrophages (TAMs), particularly CD163⁺ M2-polarized subsets, promote tumor progression, angiogenesis, and treatment resistance, correlating with lower pCR rates [26,50].

We further analyzed the model’s attention patterns in misclassified cases—where pCR was incorrectly predicted as non-pCR (false negatives) and vice versa (false positives). Figures 7 and 8 analyze false-negative (pCR misclassified as non-pCR) and false-positive (non-pCR misclassified as pCR) cases, respectively. Notably, in both scenarios, the model focused on tumor regions, validating its ability to identify tumor-specific features

relevant to NACT response. However, these examples also highlight the complexity of the TME, which can confound predictions in borderline or heterogeneous cases.

These results corroborate prior work on TME biomarkers in TNBC. For instance [51], automated tumor-infiltrating lymphocyte (TIL) assessment has shown prognostic value, while [52] combined biomarkers (e.g., TILs, Ki67, pH3) improve NACT response stratification. Similarly, [53] a combined metric of Ki-67 index (KI) and mitotic index (MI), as a superior prognostic tool for chemotherapy-treated TNBC patients compared to KI or MI alone. Given the lack of definitive histological biomarkers for pCR [25], our attention maps not only enhance interpretability but also suggest potential targets for future biomarker discovery directly from H&E images.

3.2. Significance and Clinical Implications

The ability to predict NACT response in TNBC patients has significant clinical implications [1-5]. Approximately 40–50% of TNBC patients achieve pCR, which is strongly associated with improved survival outcomes. Conversely, those with residual disease (non-pCR) face a significantly higher risk of recurrence and mortality, underscoring the value of early response prediction. Our model can aid in clinical decision-making by identifying patients likely to benefit from NACT regimens and those who may require alternative or intensified treatments. For predicted non-responders (i.e., non-pCR), this stratification could inform timely shifts to other therapeutic options or clinical trial enrollment, avoiding unnecessary toxicity from ineffective chemotherapy. For predicted responders (i.e., pCR), it could support surgical planning and reinforce adherence to current treatment pathways.

3.3. . Limitations and Future Directions

While our study demonstrates the successful prediction of NACT response in TNBC using deep learning on pre-treatment histopathological images, several limitations should be acknowledged. First, the relatively small cohort size ($n=174$), along with potential variability in digital images caused by differences in preanalytical techniques, staining methods, and scanners, may impact the generalizability of our findings despite cross-validation [54-57]. To address these challenges, future work will aim to expand the cohort size through multi-institutional collaborations for broader validation, incorporate multiplex IHC and potentially other omics data to enhance both predictive accuracy and biological insight, and pursue prospective studies to evaluate clinical utility. Ultimately, our goal is to develop reliable, personalized prediction tools for TNBC management [58-60].

4. Conclusions

In this paper, we demonstrated that deep learning applied to pre-treatment H&E-stained histopathological images can accurately predict pathologic complete response to neoadjuvant chemotherapy in triple-negative breast cancer. Analysis of the model's attention maps highlighted regions containing potential immune biomarkers, including PD-L1, CD8⁺ T-cell infiltration, and CD163⁺ macrophages. These findings underscore the potential of combining computational pathology with immune profiling to enhance both predictive accuracy and biological interpretability. Future work will focus on integrating multiplex Immunohistochemistry data, expanding to multi-institutional cohorts, and exploring novel histological biomarkers to support the development of personalized treatment strategies for TNBC patients.

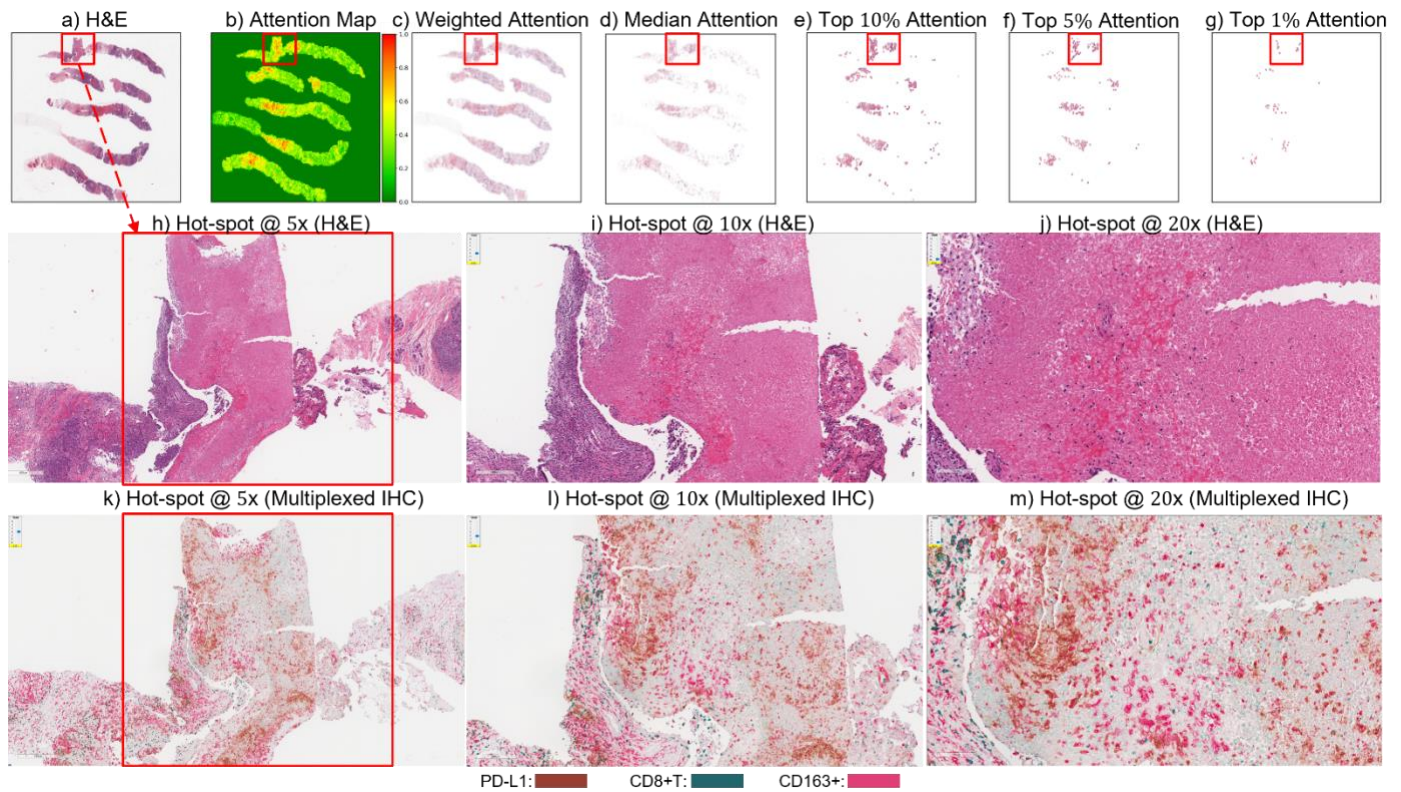


Figure 4: Attention map visualization and validation of an attention-based MIL model for a correctly classified TNBC patient (true-positive) who achieved pCR to neoadjuvant chemotherapy. (a) H&E thumbnail with (b) corresponding attention heatmap generated by the MIL model. (c) Weighted attention representation showing individual patches weighted by the model's attention scores. (d) Median attention, (e–g) Progressive filtering of attention regions showing median attention, (e) top 10% attention, (f) and top 5% attention, (g) culminating in top 1% attention hotspots. (h–j) Zoomed-in H&E images of the identified hotspot region at increasing magnifications: 5x, 10x, and 20x, respectively. (k–m) mIHC of consecutive tissue sections from the same hotspot region at corresponding magnifications (5x, 10x, 20x), revealing the presence of PD-L1 (brown), CD8+ T cells, and CD163+ macrophages (pink) in the model-identified regions. These immune markers are established biomarkers for pCR in TNBC [25], demonstrating that the model, while trained exclusively on H&E images, successfully identified immunologically regions associated with treatment response.

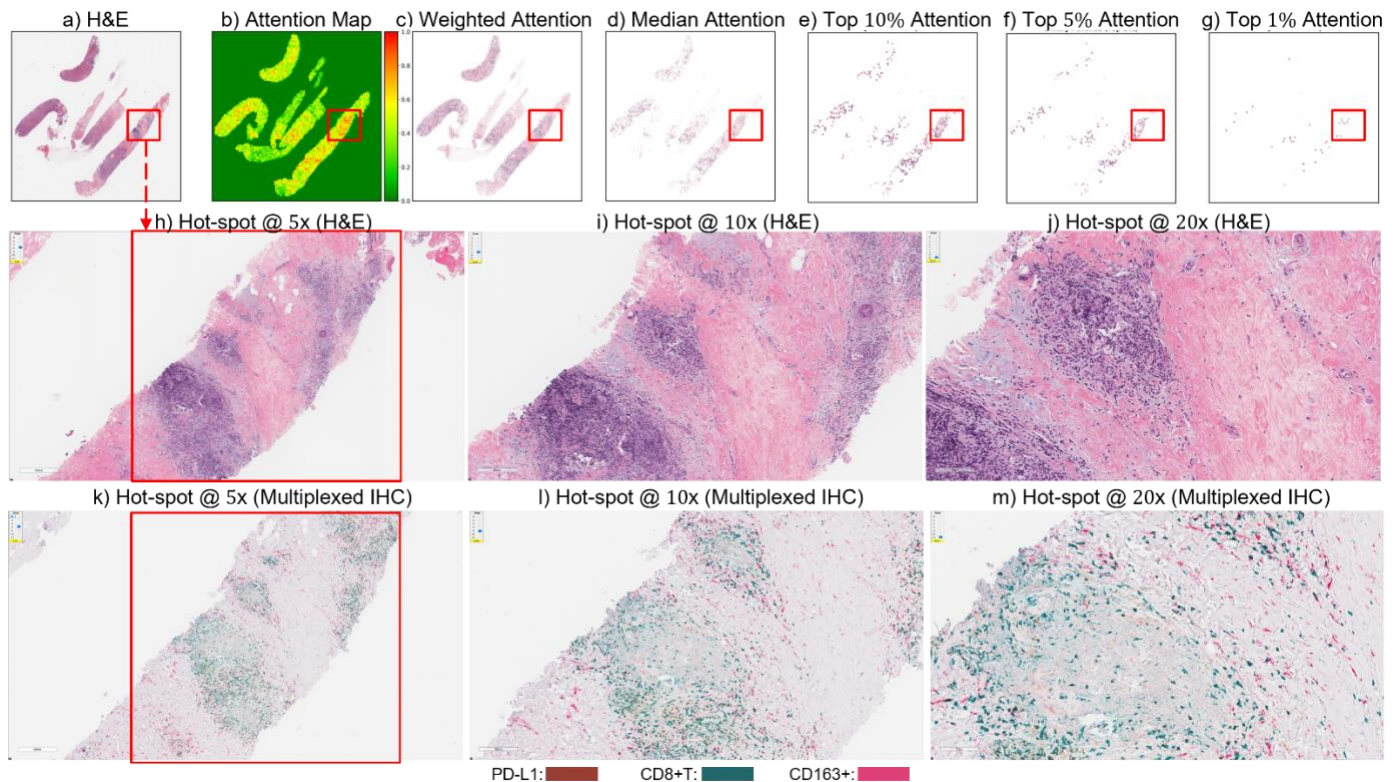


Figure 5: Attention map visualization and validation of an attention-based MIL model for a correctly classified TNBC patient (true-negative) who does not achieve pathological complete response (non-pCR) to NACT. (a) H&E thumbnail with (b) corresponding attention heatmap generated by the MIL model. (c) Weighted attention representation showing individual patches weighted by the model's attention scores. (d) Median attention, (e–g) Progressive filtering of attention regions showing median attention, (e) top 10% attention, (f) and top 5% attention, (g) culminating in top 1% attention hotspots. (h–j) Zoomed-in H&E images of the identified hotspot region at increasing magnifications: 5x, 10x, and 20x, respectively. (k–m) mIHC of consecutive tissue sections from the same hotspot region at corresponding magnifications (5x, 10x, 20x), revealing the presence of PD-L1 (brown), CD8+ T cells, and CD163+ macrophages (pink) in the model-identified regions. These immune markers are established biomarkers for pCR in TNBC [25], demonstrating that the model, while trained exclusively on H&E images, successfully identified immunologically significant tumor regions associated with treatment response.

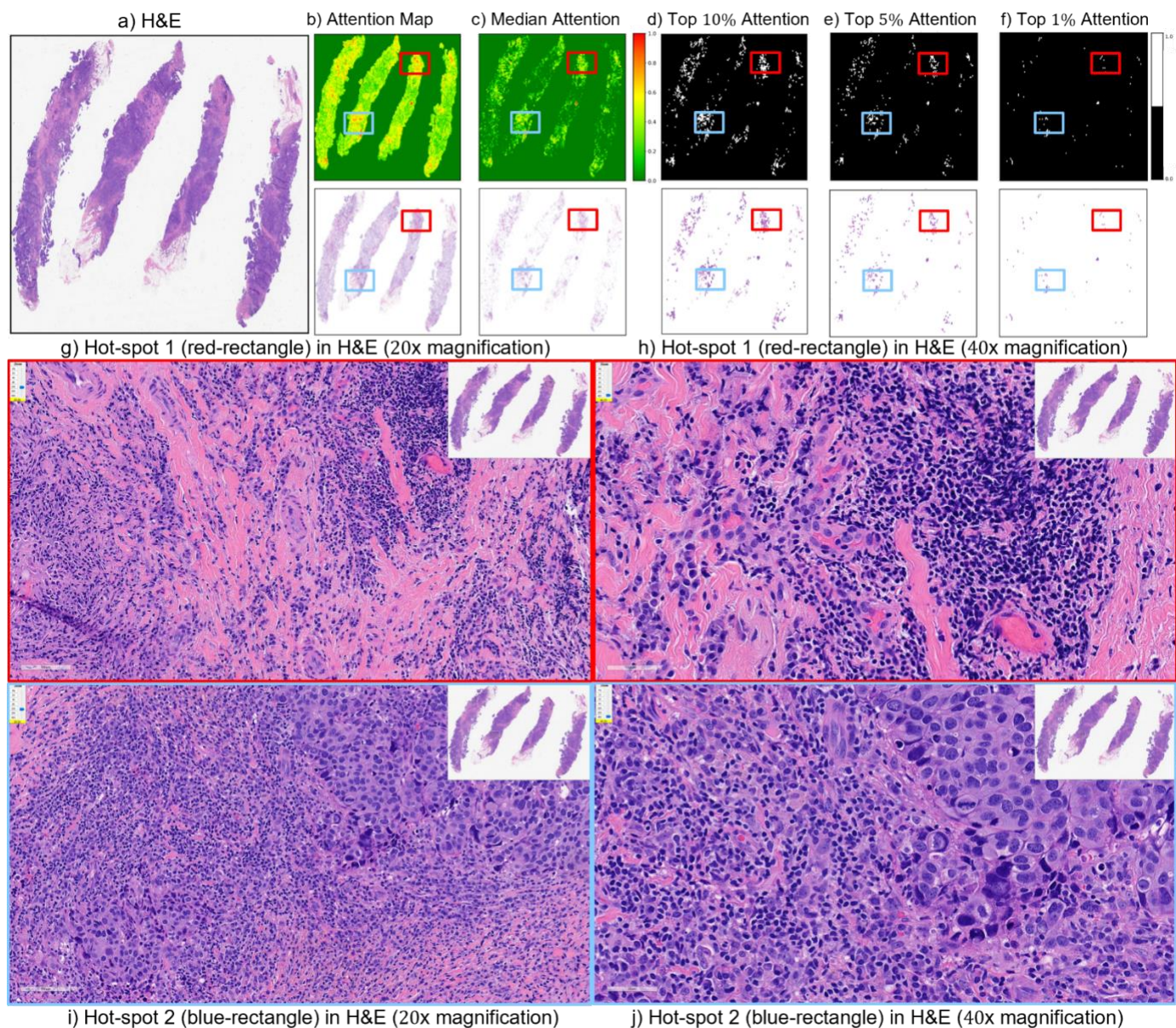


Figure 6: Attention map visualization for an incorrectly classified TNBC patient who achieved pathological complete response (pCR) to NACT, but model predicted it non-pCR. (a) H&E thumbnail (b-c) 1st row-corresponding attention heatmap generated by the deep learning model and 2nd row- display the weighted attention representation showing individual patches weighted by the model's attention scores. (c) Median attention, (d-f) displays top 10%, 5%, and 1%, attention mask while the below each mask is showing individual patches weighted by the model's attention scores. (g-h) Showing the zoomed-in H&E images of the identified hotspot region 1 (red-rectangle) at increasing magnifications of 20x, and 40x, respectively. (i-j) Showing the zoomed-in H&E images of the identified hotspot region 2 (blue rectangle) at increasing magnifications of 20x, and 40x, respectively.

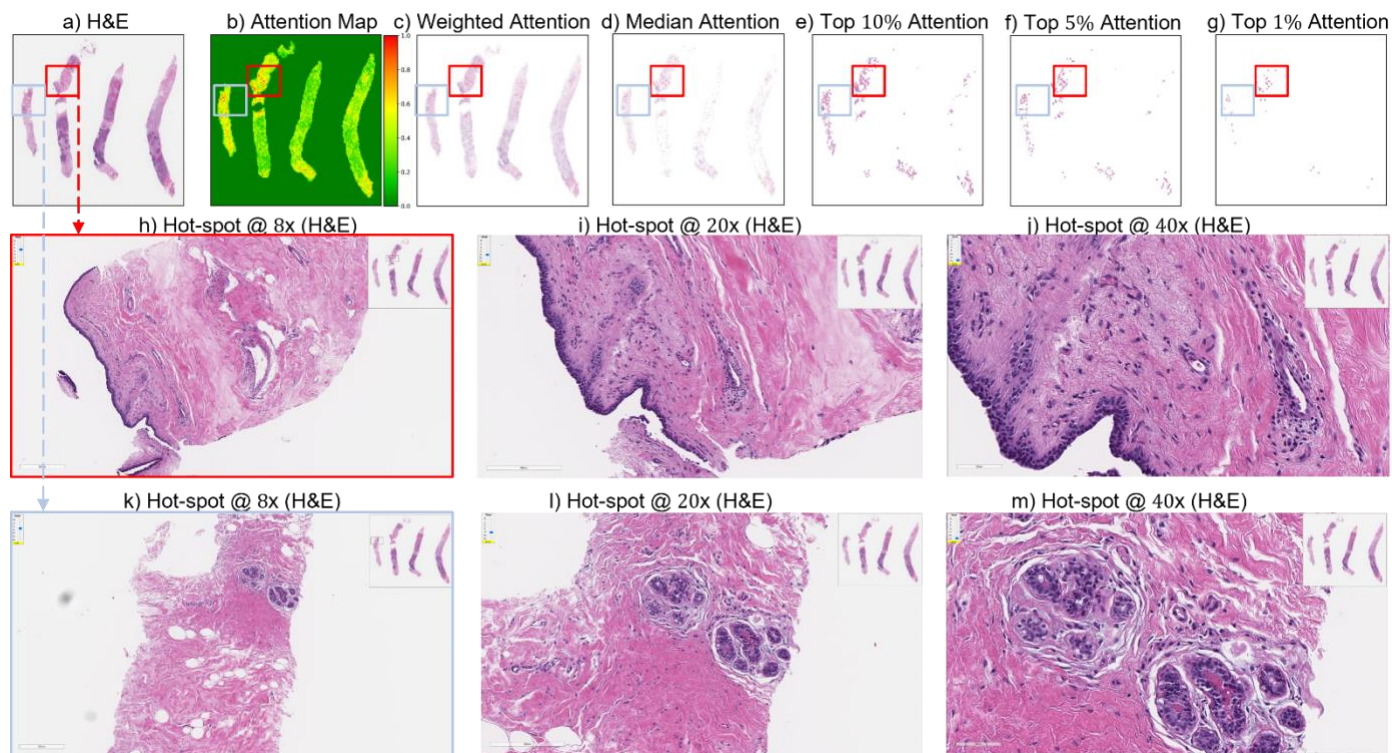


Figure 7: Attention map visualization and validation of an attention-based MIL model for an incorrectly classified TNBC patient (false-negative) who achieved pathological complete response (pCR) to NACT, but model predicted it non-pCR. (a) H&E thumbnail with (b) corresponding attention heatmap generated by the MIL model. (c) Weighted attention representation showing individual patches weighted by the model's attention scores. (d) Median attention, (e–g) Progressive filtering of attention regions showing median attention, (e) top 10% attention, (f) and top 5% attention, (g) culminating in top 1% attention hotspots. (h–k) Zoomed-in H&E images of the identified hotspot region (red-rectangle) at increasing magnifications: 8x, 20x, and 40x, respectively. (l–n) Zoomed-in H&E images of the identified hotspot region (sky-blue rectangle) at increasing magnifications: 8x, 20x, and 40x, respectively.

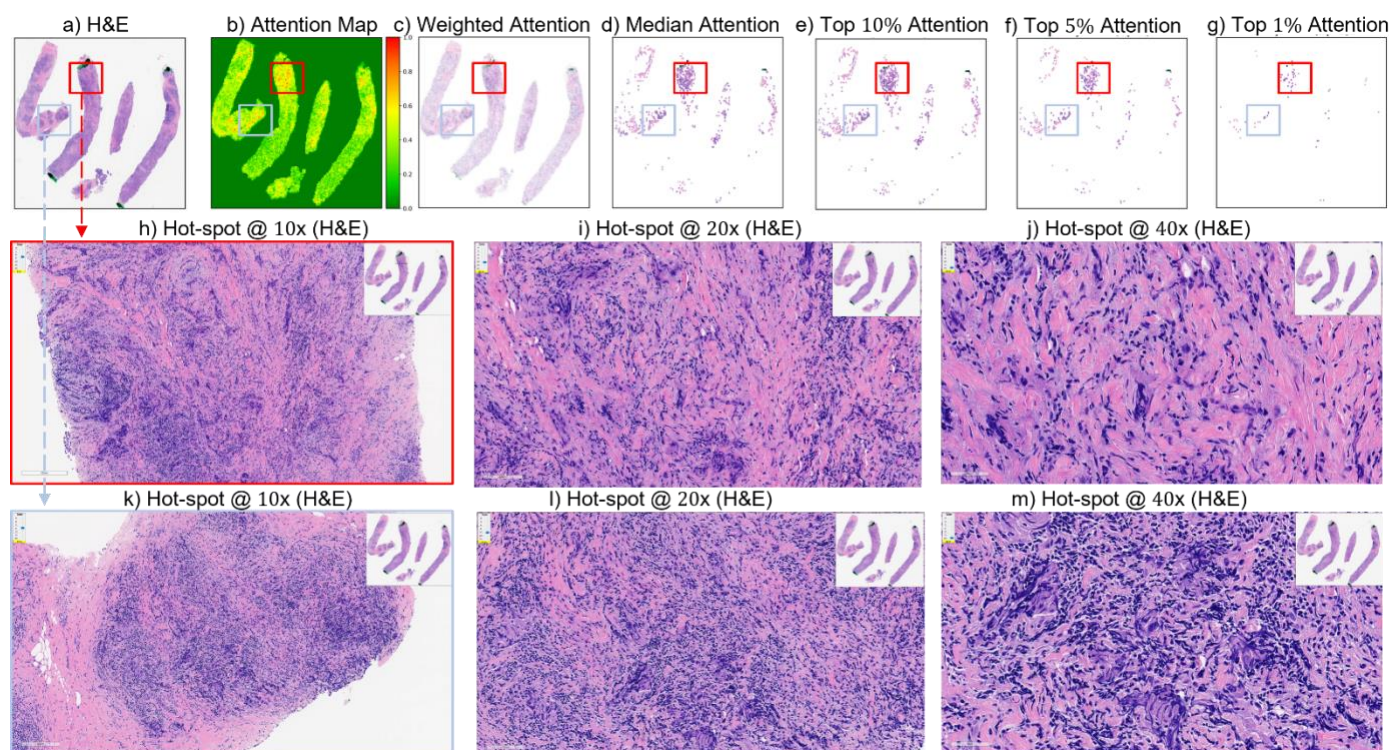


Figure 8: Attention map visualization and validation of an attention-based MIL model for a incorrectly classified TNBC patient (false-positive) who did not achieve pathological complete response (non-pCR) to NACT, but model predicted it as pCR. (a) H&E thumbnail with (b) corresponding attention heatmap generated by the MIL model. (c) Weighted attention representation showing individual patches weighted by the model's attention scores. (d) Median attention, (e–g) Progressive filtering of attention regions showing median attention, (e) top 10% attention, (f) and top 5% attention, (g) culminating in top 1% attention hotspots. (h–j) Zoomed-in H&E images of the identified hotspot region (red-rectangle) at increasing magnifications: 10x, 20x, and 40x, respectively. (k–m) Zoomed-in H&E images of the identified hotspot region (sky-blue rectangle) at increasing magnifications: 10x, 20x, and 40x, respectively.

Declaration of Competing Interest

The authors declare no competing interests.

Data sharing statement

Original data used in this study can be requested by emailing to the corresponding author Dr. Hikmat Khan at Hikmat.Khan@osumc.edu or Dr. Zaibo Li at Zaibo.Li@osumc.edu.

References

1. Soliman, A.; Li, Z.; Parwani, A.V. Artificial intelligence's impact on breast cancer pathology: a literature review. *Diagnostic pathology* 2024, 19, 38.
2. Ferlay, J.; Steliarova-Foucher, E.; Lortet-Tieulent, J.; Rosso, S.; Coebergh, J.-W.W.; Comber, H.; Forman, D.; Bray, F. Cancer incidence and mortality patterns in Europe: estimates for 40 countries in 2012. *European journal of cancer* 2013, 49, 1374-1403.
3. van den Ende, N.S.; Nguyen, A.H.; Jager, A.; Kok, M.; Debets, R.; van Deurzen, C.H. Triple-negative breast cancer and predictive markers of response to neoadjuvant chemotherapy: a systematic review. *International Journal of Molecular Sciences* 2023, 24, 2969.
4. Xiong, N.; Wu, H.; Yu, Z. Advancements and challenges in triple-negative breast cancer: A comprehensive review of therapeutic and diagnostic strategies. *Frontiers in Oncology* 2024, 14, 1405491.
5. Huang, Z.; Peng, Q.; Mao, L.; Ouyang, W.; Xiong, Y.; Tan, Y.; Chen, H.; Zhang, Z.; Li, T.; Hu, Y. Neoadjuvant Strategies for Triple Negative Breast Cancer: Current Evidence and Future Perspectives. *MedComm—Future Medicine* 2025, 4, e70013.
6. Marczyk, M.; Mrukwa, A.; Yau, C.; Wolf, D.; Chen, Y.-Y.; Balassanian, R.; Nanda, R.; Parker, B.; Krings, G.; Sattar, H. Treatment Efficacy Score—continuous residual cancer burden-based metric to compare neoadjuvant chemotherapy efficacy between randomized trial arms in breast cancer trials. *Annals of Oncology* 2022, 33, 814-823.
7. Cerbelli, B.; Scagnoli, S.; Mezi, S.; De Luca, A.; Pisegna, S.; Amabile, M.I.; Roberto, M.; Fortunato, L.; Costarelli, L.; Pernazza, A. Tissue immune profile: a tool to predict response to neoadjuvant therapy in triple negative breast cancer. *Cancers* 2020, 12, 2648.
8. Carlino, F.; Feliciano, S. Efficacy of sacituzumab govitecan in a patient with TNBC with early relapse after neoadjuvant chemotherapy. *Recenti Progressi in Medicina* 2024, 115, 26e-30e.
9. Gradishar, W.J.; Moran, M.S.; Abraham, J.; Abramson, V.; Aft, R.; Agnese, D.; Allison, K.H.; Anderson, B.; Bailey, J.; Burstein, H.J. Breast cancer, version 3.2024, NCCN clinical practice guidelines in oncology. *Journal of the National Comprehensive Cancer Network* 2024, 22, 331-357.
10. Kubouchi, K.; Shimada, K.; Yokoe, T.; Tsutsumi, Y. Avoidance and period-shortening of neoadjuvant chemotherapy against triple-negative breast cancer in stages I and II: importance of Ki-67 labeling index and the recognition of apocrine-type lesions. *Technology in Cancer Research & Treatment* 2020, 19, 1533033820943246.
11. Zhu, M.; Liang, C.; Zhang, F.; Zhu, L.; Chen, D. A nomogram to predict disease-free survival following neoadjuvant chemotherapy for triple negative breast cancer. *Frontiers in Oncology* 2021, 11, 690336.
12. Abuhadra, N.; Stecklein, S.; Sharma, P.; Moulder, S. Early-stage triple-negative breast cancer: time to optimize personalized strategies. *The oncologist* 2022, 27, 30-39.
13. Schmid, P.; Cortes, J.; Pusztai, L.; McArthur, H.; Kümmel, S.; Bergh, J.; Denkert, C.; Park, Y.H.; Hui, R.; Harbeck, N. Pembrolizumab for early triple-negative breast cancer. *New England Journal of Medicine* 2020, 382, 810-821.

14. Mittendorf, E.A.; Zhang, H.; Barrios, C.H.; Saji, S.; Jung, K.H.; Hegg, R.; Koehler, A.; Sohn, J.; Iwata, H.; Telli, M.L. Neoadjuvant atezolizumab in combination with sequential nab-paclitaxel and anthracycline-based chemotherapy versus placebo and chemotherapy in patients with early-stage triple-negative breast cancer (IMpassion031): a randomised, double-blind, phase 3 trial. *The Lancet* 2020, 396, 1090-1100.
15. Zhao, Y.; Schaafsma, E.; Cheng, C. Gene signature-based prediction of triple-negative breast cancer patient response to Neoadjuvant chemotherapy. *Cancer Medicine* 2020, 9, 6281-6295.
16. da Costa, R.E.A.R.; de Oliveira, F.T.R.; Araújo, A.L.N.; Vieira, S.C. Impact of pathologic complete response on the prognosis of triple-negative breast cancer patients: A cohort study. *Cureus* 2023, 15.
17. Bernemann, C.; Hülsewig, C.; Ruckert, C.; Schäfer, S.; Blümel, L.; Hempel, G.; Götte, M.; Greve, B.; Barth, P.J.; Kiesel, L. Influence of secreted frizzled receptor protein 1 (SFRP1) on neoadjuvant chemotherapy in triple negative breast cancer does not rely on WNT signaling. *Molecular Cancer* 2014, 13, 1-12.
18. Bianchini, G.; De Angelis, C.; Licata, L.; Gianni, L. Treatment landscape of triple-negative breast cancer—expanded options, evolving needs. *Nature reviews Clinical oncology* 2022, 19, 91-113.
19. Dent, R.; Trudeau, M.; Pritchard, K.I.; Hanna, W.M.; Kahn, H.K.; Sawka, C.A.; Lickley, L.A.; Rawlinson, E.; Sun, P.; Narod, S.A. Triple-negative breast cancer: clinical features and patterns of recurrence. *Clinical cancer research* 2007, 13, 4429-4434.
20. Oshi, M.; Newman, S.; Murthy, V.; Tokumaru, Y.; Yan, L.; Matsuyama, R.; Endo, I.; Takabe, K. ITPKC as a prognostic and predictive biomarker of neoadjuvant chemotherapy for triple negative breast cancer. *Cancers* 2020, 12, 2758.
21. Biswas, T.; Efird, J.T.; Prasad, S.; Jindal, C.; Walker, P.R. The survival benefit of neoadjuvant chemotherapy and pCR among patients with advanced stage triple negative breast cancer. *Oncotarget* 2017, 8, 112712.
22. Wimberly, H.; Brown, J.R.; Schalper, K.; Haack, H.; Silver, M.R.; Nixon, C.; Bossuyt, V.; Pusztai, L.; Lannin, D.R.; Rimm, D.L. PD-L1 expression correlates with tumor-infiltrating lymphocytes and response to neoadjuvant chemotherapy in breast cancer. *Cancer immunology research* 2015, 3, 326-332.
23. Bae, S.B.; Cho, H.D.; Oh, M.-H.; Lee, J.-H.; Jang, S.-H.; Hong, S.A.; Cho, J.; Kim, S.Y.; Han, S.W.; Lee, J.E. Expression of programmed death receptor ligand 1 with high tumor-infiltrating lymphocytes is associated with better prognosis in breast cancer. *Journal of breast cancer* 2016, 19, 242.
24. Velcheti, V.; Schalper, K.A.; Carvajal, D.E.; Anagnostou, V.K.; Syrigos, K.N.; Sznol, M.; Herbst, R.S.; Gettinger, S.N.; Chen, L.; Rimm, D.L. Programmed death ligand-1 expression in non-small cell lung cancer. *Laboratory investigation* 2014, 94, 107-116.
25. Xin, Y.; Shen, G.; Zheng, Y.; Guan, Y.; Huo, X.; Li, J.; Ren, D.; Zhao, F.; Liu, Z.; Li, Z. Immune checkpoint inhibitors plus neoadjuvant chemotherapy in early triple-negative breast cancer: a systematic review and meta-analysis. *BMC cancer* 2021, 21, 1-10.
26. Arole, V.; Nitta, H.; Wei, L.; Shen, T.; Parwani, A.V.; Li, Z. M2 tumor-associated macrophages play important role in predicting response to neoadjuvant chemotherapy in triple-negative breast carcinoma. *Breast cancer research and treatment* 2021, 188, 37-42.
27. Kim, T.; Han, W.; Kim, M.K.; Lee, J.W.; Kim, J.; Ahn, S.K.; Lee, H.-B.; Moon, H.-G.; Lee, K.-H.; Kim, T.-Y. Predictive significance of p53, Ki-67, and Bcl-2 expression for pathologic complete response after neoadjuvant chemotherapy for triple-negative breast cancer. *Journal of breast cancer* 2015, 18, 16.
28. Guestini, F.; Ono, K.; Miyashita, M.; Ishida, T.; Ohuchi, N.; Nakagawa, S.; Hirakawa, H.; Tamaki, K.; Ohi, Y.; Rai, Y. Impact of Topoisomerase II α , PTEN, ABCC1/MRP1, and Ki67 on triple-negative breast cancer patients treated with neoadjuvant chemotherapy. *Breast cancer research and treatment* 2019, 173, 275-288.
29. Mohammed, A.A.; Elsayed, F.M.; Algazar, M.; Rashed, H.E.; Anter, A.H. Neoadjuvant chemotherapy in triple negative breast cancer: correlation between androgen receptor expression and pathological response. *Asian Pacific Journal of Cancer Prevention: APJCP* 2020, 21, 563.
30. Zhu, M.; Yu, Y.; Shao, X.; Zhu, L.; Wang, L. Predictors of response and survival outcomes of triple negative breast cancer receiving neoadjuvant chemotherapy. *Chemotherapy* 2020, 65, 101-109.
31. Kedzierawski, P.; Macek, P.; Ciepiela, I.; Kowalik, A.; Gozdz, S. Evaluation of complete pathological regression after neoadjuvant chemotherapy in triple-negative breast cancer patients with brca1 founder mutation Aided Bayesian A/B testing approach. *Diagnostics* 2021, 11, 1144.
32. Bignon, L.; Fricker, J.P.; Nogues, C.; Mouret-Fourme, E.; Stoppa-Lyonnet, D.; Caron, O.; Lortholary, A.; Faivre, L.; Lasset, C.; Mari, V. Efficacy of anthracycline/taxane-based neo-adjuvant chemotherapy on triple-negative breast cancer in BRCA 1/BRCA 2 mutation carriers. *The breast journal* 2018, 24, 269-277.

33. Masuda, H.; Masuda, N.; Kodama, Y.; Ogawa, M.; Karita, M.; Yamamura, J.; Tsukuda, K.; Doihara, H.; Miyoshi, S.; Mano, M. Predictive factors for the effectiveness of neoadjuvant chemotherapy and prognosis in triple-negative breast cancer patients. *Cancer chemotherapy and pharmacology* 2011, 67, 911-917.
34. Van Bockstal, M.R.; Noel, F.; Guiot, Y.; Duhoux, F.P.; Mazzeo, F.; Van Marcke, C.; Fellah, L.; Ledoux, B.; Berlière, M.; Galant, C. Predictive markers for pathological complete response after neo-adjuvant chemotherapy in triple-negative breast cancer. *Annals of Diagnostic Pathology* 2020, 49, 151634.
35. Zhou, Z.; Adrada, B.E.; Candelaria, R.P.; Elshafeey, N.A.; Boge, M.; Mohamed, R.M.; Pashapoor, S.; Sun, J.; Xu, Z.; Panthi, B. Prediction of pathologic complete response to neoadjuvant systemic therapy in triple negative breast cancer using deep learning on multiparametric MRI. *Scientific reports* 2023, 13, 1171.
36. Golden, D.I.; Lipson, J.A.; Telli, M.L.; Ford, J.M.; Rubin, D.L. Dynamic contrast-enhanced MRI-based biomarkers of therapeutic response in triple-negative breast cancer. *Journal of the American Medical Informatics Association* 2013, 20, 1059-1066.
37. Jiang, M.; Li, C.-L.; Luo, X.-M.; Chuan, Z.-R.; Lv, W.-Z.; Li, X.; Cui, X.-W.; Dietrich, C.F. Ultrasound-based deep learning radiomics in the assessment of pathological complete response to neoadjuvant chemotherapy in locally advanced breast cancer. *European Journal of Cancer* 2021, 147, 95-105.
38. Xu, Z.; Zhou, Z.; Son, J.B.; Feng, H.; Adrada, B.E.; Moseley, T.W.; Candelaria, R.P.; Guirguis, M.S.; Patel, M.M.; Whitman, G.J. Deep Learning Models Based on Pretreatment MRI and Clinicopathological Data to Predict Responses to Neoadjuvant Systemic Therapy in Triple-Negative Breast Cancer. *Cancers* 2025, 17, 966.
39. Jimenez, J.E.; Abdelhafez, A.; Mittendorf, E.A.; Elshafeey, N.; Yung, J.P.; Litton, J.K.; Adrada, B.E.; Candelaria, R.P.; White, J.; Thompson, A.M. A model combining pretreatment MRI radiomic features and tumor-infiltrating lymphocytes to predict response to neoadjuvant systemic therapy in triple-negative breast cancer. *European Journal of Radiology* 2022, 149, 110220.
40. Krishnamurthy, S.; Jain, P.; Tripathy, D.; Basset, R.; Randhawa, R.; Muhammad, H.; Huang, W.; Yang, H.; Kummar, S.; Wilding, G. Predicting response of triple-negative breast cancer to neoadjuvant chemotherapy using a Deep convolutional neural network-based artificial intelligence tool. *JCO Clinical Cancer Informatics* 2023, 7, e2200181.
41. Huang, Z.; Shao, W.; Han, Z.; Alkashash, A.M.; De la Sancha, C.; Parwani, A.V.; Nitta, H.; Hou, Y.; Wang, T.; Salama, P. Artificial intelligence reveals features associated with breast cancer neoadjuvant chemotherapy responses from multi-stain histopathologic images. *NPJ Precision Oncology* 2023, 7, 14.
42. Hussain, M.S.; Ramalingam, P.S.; Chellamy, G.; Yun, K.; Bisht, A.S.; Gupta, G. Harnessing Artificial Intelligence for Precision Diagnosis and Treatment of Triple Negative Breast Cancer. *Clinical Breast Cancer* 2025.
43. Ilse, M.; Tomczak, J.; Welling, M. Attention-based deep multiple instance learning. In *Proceedings of the International conference on machine learning*, 2018; pp. 2127-2136.
44. Chen, R.J.a.D.T.a.L.M.Y.a.W.D.F.K.a.J.G.a.S.A.H.a.C.B.a.Z.A.a.; et al. Towards a general-purpose foundation model for computational pathology. *Nature Medicine* 2024, 30, 850-862.
45. Bilal, M.; Raza, M.; Altherwy, Y.; Alsuhaibani, A.; Abduljabbar, A.; Almarshad, F.; Golding, P.; Rajpoot, N. Foundation Models in Computational Pathology: A Review of Challenges, Opportunities, and Impact. *arXiv preprint arXiv:2502.08333* 2025.
46. Bottou, L. Stochastic gradient descent tricks. In *Neural networks: tricks of the trade: second edition*; Springer: 2012; pp. 421-436.
47. Ketkar, N. Stochastic gradient descent. In *Deep learning with Python: A hands-on introduction*; Springer: 2017; pp. 113-132.
48. Wang, Z.; Wang, P.; Liu, K.; Wang, P.; Fu, Y.; Lu, C.-T.; Aggarwal, C.C.; Pei, J.; Zhou, Y. A comprehensive survey on data augmentation. *arXiv preprint arXiv:2405.09591* 2024.
49. Faryna, K.; van der Laak, J.; Litjens, G. Automatic data augmentation to improve generalization of deep learning in H&E stained histopathology. *Computers in Biology and Medicine* 2024, 170, 108018.
50. Ye, J.-h.; Wang, X.-h.; Shi, J.-j.; Yin, X.; Chen, C.; Chen, Y.; Wu, H.-Y.; Jiong, S.; Zhang, M.; Shi, X.-b. Tumor-associated macrophages are associated with response to neoadjuvant chemotherapy and poor outcomes in patients with triple-negative breast cancer. *Journal of Cancer* 2021, 12, 2886.
51. Baharun, N.B.; Adam, A.; Zailani, M.A.H.; Rajpoot, N.M.; Xu, Q.; Zin, R.R.M. Automated scoring methods for quantitative interpretation of Tumour infiltrating lymphocytes (TILs) in breast cancer: a systematic review. *BMC cancer* 2024, 24, 1202.
52. Bhattarai, S.; Saini, G.; Li, H.; Seth, G.; Fisher, T.B.; Janssen, E.A.; Kiraz, U.; Kong, J.; Aneja, R. Predicting neoadjuvant treatment response in triple-negative breast cancer using machine learning. *Diagnostics* 2023, 14, 74.

53. Bhattarai, S.; Rupji, M.; Chao, H.-p.; Xu, Q.; Saini, G.; Rida, P.; Aleskandarany, M.A.; Green, A.R.; Ellis, I.O.; Janssen, E.A. Cell cycle traverse rate predicts long-term outcomes in a multi-institutional cohort of patients with triple-negative breast cancer. *BJC reports* 2024, 2, 87.
54. Abele, N.; Tiemann, K.; Krech, T.; Wellmann, A.; Schaaf, C.; Länger, F.; Peters, A.; Donner, A.; Keil, F.; Daifalla, K. Noninferiority of artificial intelligence–assisted analysis of Ki-67 and estrogen/progesterone receptor in breast cancer routine diagnostics. *Modern Pathology* 2023, 36, 100033.
55. Cruz-Roa, A.; Gilmore, H.; Basavanahally, A.; Feldman, M.; Ganesan, S.; Shih, N.; Tomaszewski, J.; Madabhushi, A.; González, F. High-throughput adaptive sampling for whole-slide histopathology image analysis (HASHI) via convolutional neural networks: Application to invasive breast cancer detection. *PloS one* 2018, 13, e0196828.
56. Hartage, R.; Li, A.C.; Hammond, S.; Parwani, A.V. A validation study of human epidermal growth factor receptor 2 immunohistochemistry digital imaging analysis and its correlation with human epidermal growth factor receptor 2 fluorescence in situ hybridization results in breast carcinoma. *Journal of pathology informatics* 2020, 11, 2.
57. Li, A.C.; Zhao, J.; Zhao, C.; Ma, Z.; Hartage, R.; Zhang, Y.; Li, X.; Parwani, A.V. Quantitative digital imaging analysis of HER2 immunohistochemistry predicts the response to anti-HER2 neoadjuvant chemotherapy in HER2-positive breast carcinoma. *Breast cancer research and treatment* 2020, 180, 321-329.
58. Lee, H.-j.; Lee, J.H.; Lee, J.E.; Na, Y.M.; Park, M.H.; Lee, J.S.; Lim, H.S. Prediction of early clinical response to neoadjuvant chemotherapy in Triple-negative breast cancer: Incorporating Radiomics through breast MRI. *Scientific Reports* 2024, 14, 21691.
59. Wang, G.; Yao, Y.; Huang, H.; Zhou, J.; Ni, C. Multiomics technologies for comprehensive tumor microenvironment analysis in triple-negative breast cancer under neoadjuvant chemotherapy. *Frontiers in Oncology* 2023, 13, 1131259.
60. Tang, X.; Thompson, K.J.; Kalari, K.R.; Sinnwell, J.P.; Suman, V.J.; Vedell, P.T.; McLaughlin, S.A.; Northfelt, D.W.; Aspitia, A.M.; Gray, R.J. Integration of multiomics data shows down regulation of mismatch repair and tubulin pathways in triple-negative chemotherapy-resistant breast tumors. *Breast Cancer Research* 2023, 25, 57.